Chen, Kexun; Setälä, Olli; Liu, Xiaolong; Radfar, Behrad; Pasanen, Toni; Serue, Michael; Heinonen, Juha; Savin, Hele; Vähänissi, Ville

Excellent Responsivity and Low Dark Current Obtained with Metal-Assisted Chemical Etched Si Photodiode

Published in:
IEEE Sensors Journal

DOI:
10.1109/JSEN.2023.3246505

Published: 01/04/2023

Document Version
Publisher's PDF, also known as Version of record

Please cite the original version:
Chen, K., Setälä, O., Liu, X., Radfar, B., Pasanen, T., Serue, M., Heinonen, J., Savin, H., & Vähänissi, V. (2023). Excellent Responsivity and Low Dark Current Obtained with Metal-Assisted Chemical Etched Si Photodiode. *IEEE Sensors Journal*, *23*(7), 6750-6756. https://doi.org/10.1109/JSEN.2023.3246505

IEEE Sensors Council

Excellent Responsivity and Low Dark Current Obtained With Metal-Assisted Chemical Etched Si Photodiode

Kexun Chen, Olli E. Setälä, Xiaolong Liu, Behrad Radfar, *Graduate Student Member, IEEE*, Toni P. Pasanen, Michael D. Serué, Juha Heinonen, Hele Savin, and Ville Vähänissi

***Abstract*—Metal-assisted chemical etched (MACE; also known as MacEtch or MCCE) nanostructures are utilized widely in the solar cell industry due to their excellent optical properties combined with a simple and cost-efficient fabrication process. The photodetection community, on the other hand, has not shown much interest toward MACE due to its drawbacks, including insufficient surface passivation, increased junction recombination, and possible metal contamination, which are especially detrimental to p-n photodiodes. Here, we aim to change this by demonstrating how to fabricate high-performance MACE p-n photodiodes with above 90% external quantum efficiency (EQE) without external bias voltage at 200–1000 nm and dark current less than 3 nA/cm^2 at −5 V using industrially applicable methods. The key is to utilize an induced junction created by an atomic layer deposited (ALD) highly charged Al_2O_3 thin film that simultaneously provides efficient field-effect passivation and full conformality over the MACE nanostructures. Achieving close to ideal performance demonstrates the vast potential of MACE nanostructures in the fabrication of high-performance low-cost p-n photodiodes.**

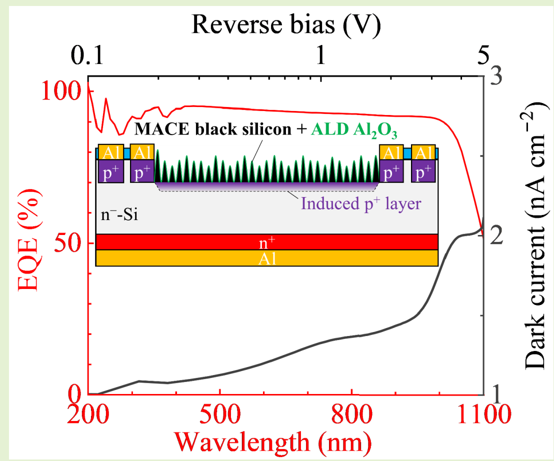

***Index Terms*— MACE, photodetector, responsivity, Si.**

I. Introduction

SILICON-BASED p-n photodiodes that convert incident light to an electrical signal are extensively used in a wide range of commercial applications ranging from telecommunication to medical sensing and imaging and from consumer wearables to self-driving vehicles—just to name a few [1], [2], [3], [4]. To achieve high performance, namely, high sensitivity, from a p-n photodiode, minimizing reflection and recombination losses is of vital importance. In that sense, high-performance p-n photodiodes resemble high-efficiency Si solar cells [5], [6], although there are obviously some differences in, e.g., operating voltages and signal levels.

In state-of-the-art silicon solar cells, the reflectance losses have been mitigated by utilizing surface nanostructures [i.e., black silicon (b-Si)], which enable a drastic decrease in total reflectance (R) over a wide wavelength range (200–1000 nm) [7], [8], [9]. While there are different methods for the fabrication of surface nanostructures, in photovoltaics, the metal-assisted chemical etching (MACE; also known as MacEtch or MCCE) technique has turned out to be the most attractive, as it is a simple, cost-efficient, and crystal-damage-free process that has been shown to be easy to scale-up industrially [10], [11], [12], [13], [14], [15]. MACE should, therefore, offer an attractive means to reduce the reflectance losses also in industrial photodiodes.

The second key factor for achieving a high-sensitivity p-n photodiode is the reduction of carrier recombination.

Manuscript received 29 December 2022; revised 2 February 2023; accepted 5 February 2023. Date of publication 24 February 2023; date of current version 31 March 2023. This work was supported in part by the Academy of Finland under Grant 331313, in part by the Business Finland through Project FemtoBlack under Grant 7479/31/2019, in part by the Tandem Industry Academia from the Finnish Research Impact Foundation, in part by the EMPIR Program co-financed by the Participating States and from the European Union's Horizon 2020 Research and Innovation Program (NanoWires) under Project 19ENG05, and in part by the Flagship on Photonics Research and Innovation "PREIN" funded by the Academy of Finland. The associate editor coordinating the review of this article and approving it for publication was Prof. Hsin-Ying Lee. *(Corresponding author: Kexun Chen.)*

Kexun Chen, Olli E. Setälä, Xiaolong Liu, Behrad Radfar, Toni P. Pasanen, Hele Savin, and Ville Vähänissi are with the Department of Electronics and Nanoengineering, Aalto University, 02150 Espoo, Finland (e-mail: kexun.1.chen@aalto.fi; olli.setala@aalto.fi; xiaolong.liu@aalto.fi; behrad.radfar@aalto.fi; toni.pasanen@aalto.fi; hele.savin@aalto.fi; ville.vahanissi@aalto.fi).

Michael D. Serué and Juha Heinonen are with ElFys, Inc., 02150 Espoo, Finland (e-mail: michael.serue@elfys.fi; juha.heinonen@elfys.fi).

Digital Object Identifier 10.1109/JSEN.2023.3246505

Recombination in the Si bulk can be minimized by using high-quality substrates and avoiding contamination during semiconductor processing. Surface recombination can be suppressed by utilizing the so-called field-effect passivation by a highly charged atomic layer deposited (ALD) Al_2O_3 film [16], [17]. This method has been introduced already in 2006 [18] and is nowadays commercially exploited, e.g., in Si solar cells. An additional benefit of ALD is that it forms a highly conformal and stable coating [19], [20], [21], and thus, the method works well also on nanostructured surfaces [16]. More specifically, for MACE nanostructures, we have previously reported [22] a high effective carrier lifetime of ≈400 μs (at an injection level of 10^{15} cm^{-3}) using ALD Al_2O_3 passivation while keeping the surface reflectivity as low as 3.9% in the wavelength range of 300–1000 nm. After further development, even millisecond-range lifetimes were reached, indicating that MACE causes no contamination to Si bulk. Such high carrier lifetimes should fulfill the strict requirement for low dark current in photodiodes.

An additional source of recombination is the charge-collecting p-n junction that is traditionally fabricated via external doping, such as ion implantation or dopant diffusion. A high concentration of dopants results in increased Auger recombination inside the junction, and implantation may cause crystal damage that is not fully recovered during subsequent annealing. In p-n photodiodes, the dopant-related recombination source can be mitigated by replacing the external doping with a built-in inversion layer, which forms underneath the same charged ALD Al_2O_3 film that is used for surface passivation [23]. In solar cells, such an inversion layer would cause too high resistive losses due to a much higher current density, but in photodiodes, the inversion layer can boost the performance especially at short wavelengths, which are absorbed inside the junction [24], [25]. So far, the integration of such an ALD-based inversion layer with MACE nanostructures has not yet been reported, but it could be the key to raising the performance of MACE photodiodes to a completely new level.

While MACE has previously been applied to Schottky photodiodes [26], [27], it is well known that they always suffer from high dark current and, consequently, have limited sensitivity. For instance, Zhang et al. [26] have recently reported a high-responsivity MACE Si Schottky photodiode; however, the achieved dark current density is as high as 130 nA cm^{-2} at −1-V bias, which cannot compete with commercial Si photodiodes (typically <10 nA cm^{-2}). Unlike Schottky diodes, p-n diodes are known for their low dark currents. However, there are only limited investigations made on MACE p-n photodiodes (e.g., by Zhong et al. [28]), and the obtained results have left room for improvement, falling clearly below the commercial counterparts [24], [29]. Thus, we believe that the full potential of MACE in p-n photodiode manufacturing has not yet been demonstrated.

In this article, our aim is to demonstrate a high-performance Si p-n photodiode by utilizing industrially feasible MACE nanostructures together with ALD Al_2O_3 that reduces surface recombination and simultaneously induces an inversion layer forming a charge collecting junction. We characterize the spectral responsivity (R_λ) of the photodiodes in a wide wavelength range and compare the results to the existing literature. We analyze the results considering separately the optical and recombination losses along with other typical figures of merit, such as dark current and detectivity. Finally, the potential of using MACE in fabrication of high-performance commercial photodiodes is discussed.

II. Experimental Section

Fig. 1(a) presents a photograph of the fabricated MACE b-Si p-n photodiode. Several MACE b-Si and reference planar devices with a circular active area with a radius of 2.5 mm were fabricated on a 380-μm-thick 4-in n-type float-zone Si wafer with a resistivity of >9000 Ω cm and a (111) orientation. The fabrication of the MACE b-Si devices is described next, while the planar reference devices follow the exact same steps excluding the actual MACE process. First, the wafer was treated at 1000 °C under an O_2 atmosphere for 84 min to grow ≈500-nm SiO_2 on the surfaces by wet oxidation. The oxide layer was patterned by photolithography and used as a mask material for the following ion implantation. Boron (B) and phosphorus (P) implantations were used to form highly doped areas allowing ohmic contact between the Si bulk and the contact metals on the front and rear sides of the wafer, respectively. The front opening areas were implanted with a B dose of 1×10^{15} cm^{-2} and an ion energy of 33 keV, while the whole rear surface was implanted with a P dose of 2×10^{15} cm^{-2} and an ion energy of 50 keV. The implantation was followed by a SiO_2 removal and drive-in for the dopants at 1000 °C for 50 min. A new SiO_2 layer was grown during the drive-in step, which served as an etching mask during the MACE process; i.e., the SiO_2 layer was removed locally only from the b-Si (or planar) active device areas. Next, a two-step room temperature MACE process was used to form b-Si nanostructures. The etching parameters were chosen based on our earlier work [22] to optimize the electrical and optical properties of the final devices. First, the wafer was dipped in a solution of HF (50 wt%) 80 mL, $AgNO_3$ (0.005 mol/L) 400 mL, and H_2O 400 mL for 20 s to deposit Ag nanoparticles on the surface. Second, the wafer was etched in a solution of HF (50 wt%) 150 mL, H_2O_2(30 wt%) 100 mL, and H_2O 2700 mL for 3 min to form surface nanostructures. Afterward, the Ag nanoparticles were removed in 69-wt% HNO_3 for 15 min. Fig. 1(b) shows a scanning electron microscope (SEM) image of the resulting nanostructures after Ag removal. The average diameter and height of the nanostructures measured by SEM were ≈0.25 and ≈1.5 μm, respectively.

A 50-nm Al_2O_3 layer was deposited with Beneq TFS-500 ALD reactor on the nanostructures at a temperature of 200 °C with trimethylaluminum and water as precursors. The negatively charged Al_2O_3 film passivates the nanostructured surface and generates the p^+ inversion layer into the lowly doped n-type substrate, as demonstrated in Fig. 1(c). The Al_2O_3 film was then patterned with photolithography to make the contact openings for the front metal contacts. Subsequently, 300- and 500-nm-thick Al layers were deposited by the MRC 903 sputtering system on the front- and rear-doped surface regions, respectively. This was followed again

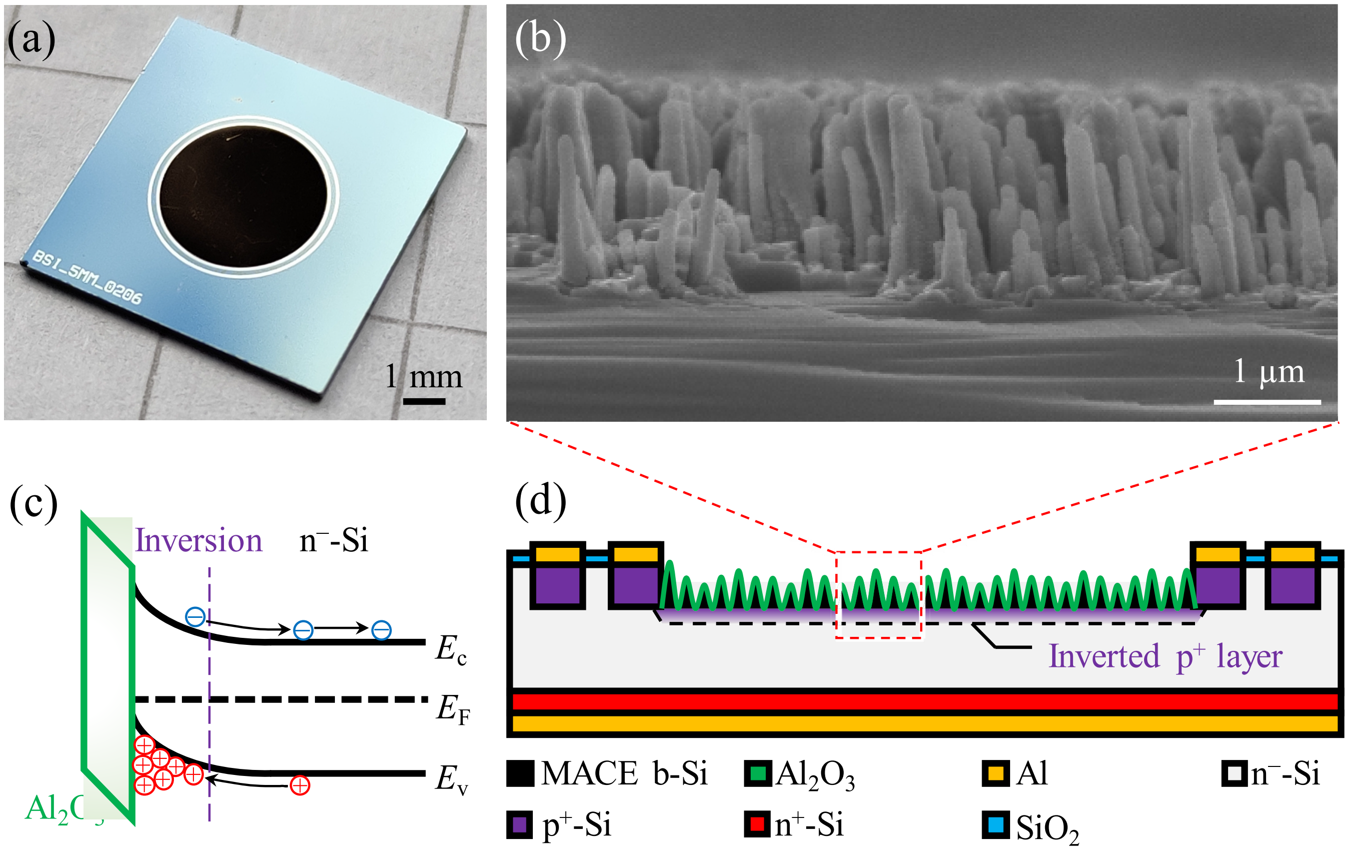

Fig. 1. (a) Photograph of the MACE b-Si photodiode. (b) SEM image showing the MACE b-Si morphology. (c) Energy band diagram of the lowly doped n-type Si covered by a highly negative-charged Al_2O_3. (d) Detailed device cross section.

with photolithography to pattern the front contacts. Finally, the wafers were annealed at 425 °C for 20 min in forming gas to activate the Al_2O_3 passivation and to sinter the Al contacts. The cross section of the final MACE device is presented in Fig. 1(d). The cross section of the planar reference device is alike apart from the MACE b-Si structures.

For determining the external quantum efficiency (EQE), the photodiodes were attached to a printed circuit board and placed in a dark box sealed from room lighting. The used light source was Bentham ILD-D2-QH-24, which was directly coupled to the entrance port of a Bentham TMC300_0060 monochromator. The monochromator was used to select the wavelength (200–1100 nm) with 10-nm bandwidth, and the resulting beam was focused on the sample surface using lens-based relay optics. The light beam was first aligned perpendicular to the diode front surface, and the light-generated output current of the photodiodes was measured as a function of wavelength. Subsequently, the output current was transformed into EQE by calibrating the values against a b-Si detector, which had been calibrated using standards traceable to the Physikalisch-Technische Bundesanstalt (PTB) [25]. The corresponding spectral responsivity was calculated with $R_\lambda = \mathrm{EQE}_\lambda \times (q\lambda/hc)$, where q is the elementary charge, h the Planck constant, and λ and c the wavelength and speed of light, respectively.

The total reflectance was characterized between 250 and 1100 nm with a Cary 5000 UV–Vis–NIR spectrophotometer equipped with an integrating sphere. In addition, the homogeneity of the reflectance was characterized at the wavelengths of 656 and 984 nm using a PV2000A metrology tool (SEMILAB SDI) with a spot size of 100 μm. The internal quantum efficiency (IQE) was determined from the EQE and total reflectance measurements. Dark I–V curves were measured by a Hewlett–Packard Model 4145A semiconductor parameter analyzer. Finally, the specific detectivity (D^*) was calculated, assuming that the dark current is the dominating noise source using the equation [30], [31], $D^* = R_\lambda((A/2qI_D))^{1/2}$, where A is the active area of the detector, and I_D is the dark current.

III. Results and Discussion

Fig. 2(a) and (b) presents the spectral responsivity and the EQE of our MACE and planar reference photodiodes measured at zero bias voltage. These parameters illustrate how well the photodiode detects the light signal: the former describes the amount of output current per incident power at a given wavelength, and the latter describes the probability at which the incoming photon will be transferred to a current signal. As shown in Fig. 2, our MACE photodiode exhibits excellent responsivity (and EQE) for a wide wavelength range of 200–1000 nm, and the values are well above those reported previously for MACE photodiodes. Note also that when the wavelength of the incoming photon is 200 nm, the responsivity exceeds even the theoretical one electron per one photon limit raising the EQE to ≈102%. The phenomenon related to the

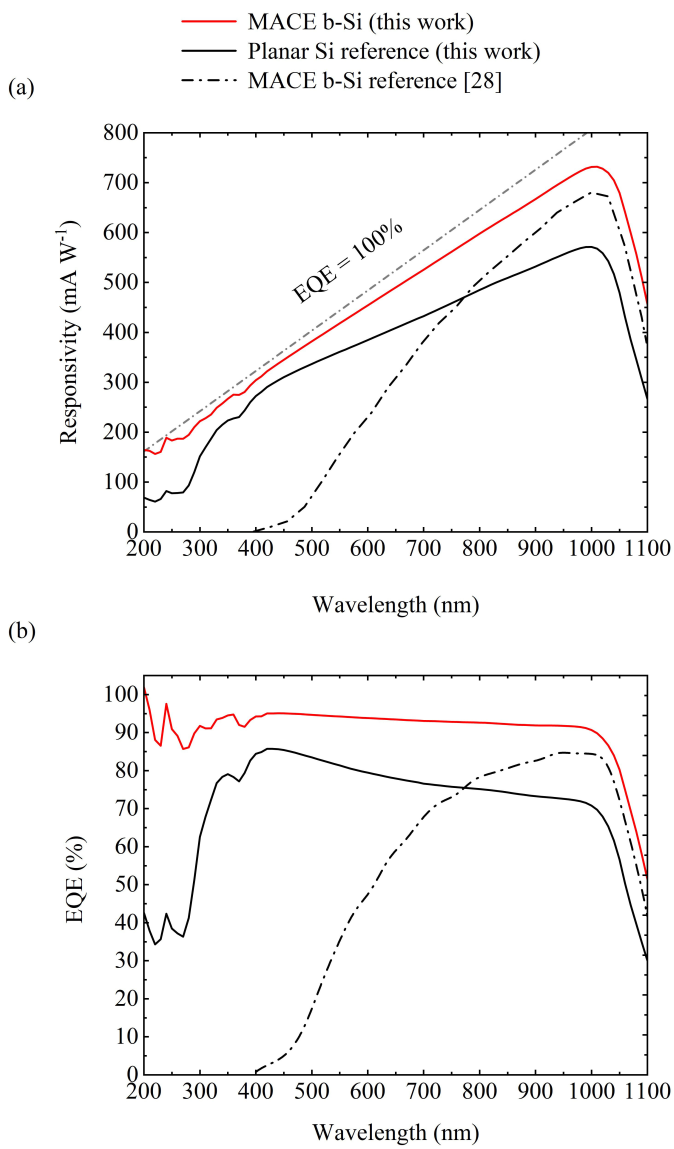

Fig. 2. (a) Spectral responsivity and (b) EQE of the MACE b-Si and planar Si photodiodes fabricated in this work measured at zero bias, and as a comparison, a state-of-the-art MACE p-n photodiode measured at –12-V bias [28].

above unity EQE has been previously correlated with impact ionization; i.e., the UV photons have a high enough energy to excite multiple electron–hole pairs without the presence of an external bias voltage [32]. This phenomenon can be observed only in devices that have low enough recombination rates. The planar counterpart shows rather high responsivity as well, especially around 400 nm, but is still clearly below the performance of the MACE photodiode. This is because a single layer of Al_2O_3 (50-nm thick) cannot provide similar antireflection performance to the MACE surface.

As a further comparison, the performance of a state-of-the-art MACE p-n photodiode [28] is also included in Fig. 2. It is apparent that this photodiode performs best at near-infrared (NIR) wavelengths. However, it can reach a similar level to our MACE photodiode only in a rather narrow wavelength range (1000–1100 nm). Note that our and the reference MACE photodiodes have been measured at different reverse bias voltages (0 versus –12 V). We would expect an increase, albeit a minor one, in the responsivity of our device when measured at higher biases due to more efficient charge collection.

In order to explain the much higher performance of our MACE photodiode compared with the previous work, we analyze the optical and recombination properties as well as the dark current of the diodes. We start by examining the optical properties, namely, the total reflectance [Fig. 3(a)]. It can be seen that the reflectance in our MACE nanostructured surface is rather constant (≈5%) in the whole wavelength range (250–1100 nm). Fig. 3(a) (inset) confirms that the reflectance of our MACE photodiode is also highly uniform spatially. The uniformity at both 656 and 984 nm is approximately ±1.2% absolute (note that the small difference between the absolute values of spectral and spatial reflectance is due to two different characterization tools). As expected, in the planar photodiode, the reflectance is much higher as compared with MACE surfaces and reaches its minimum value (≈13%) near 400 nm correlating with the antireflection effect produced by a 50-nm-thick Al_2O_3 on planar Si surface. The reflectance curve of the reference MACE photodiode [28] is relatively flat and in the same range as our MACE photodiode. Therefore, the reflectance cannot explain the difference in responsivity between the two MACE photodiodes.

As mentioned in Section I, it is important to also analyze the possible recombination losses in the photodiode. This is best done via IQE, which disregards the reflection losses and, thus, describes how many electrons can be collected to the contacts per the number of absorbed photons. In other words, the IQE is a direct measure of recombination activity. Fig. 3(b) presents the IQE of our MACE and planar photodiodes as well as the reference MACE photodiode. The IQE of our MACE photodiode is close to ideal (100%) in a wide wavelength region confirming that it does not considerably suffer from either surface or bulk recombination. This is because we have used the following: 1) a high bulk lifetime substrate; 2) ALD Al_2O_3 surface passivation; and 3) a low-recombination inversion layer as the charge collecting junction. It is worth highlighting that the high IQE in a wide wavelength range also proves that MACE is not a significant source of (metal) contamination to the wafers. In addition, it is worth noting that our planar photodiode also exhibits near perfect IQE, and in the UV (250–400 nm), the planar device even outperforms the MACE photodiode. This means that in MACE, the surface recombination is higher than in the planar surface, which is a reasonable result considering the higher surface area related to the nanostructures.

The nanostructures of the reference MACE photodiode were not passivated, and the p-n junction was formed by dopant diffusion. Both issues are likely to cause severe recombination losses near the front surface, and thus, these factors explain the resulting negligible IQE in UV. In the longer wavelength region (800–1000 nm), both our and reference MACE photodiodes result in relatively high IQE. Since these longer wavelengths are absorbed mostly deep in the Si bulk, the IQE results confirm that bulk or the rear surface recombinations are not significantly limiting the device performance in either MACE device.

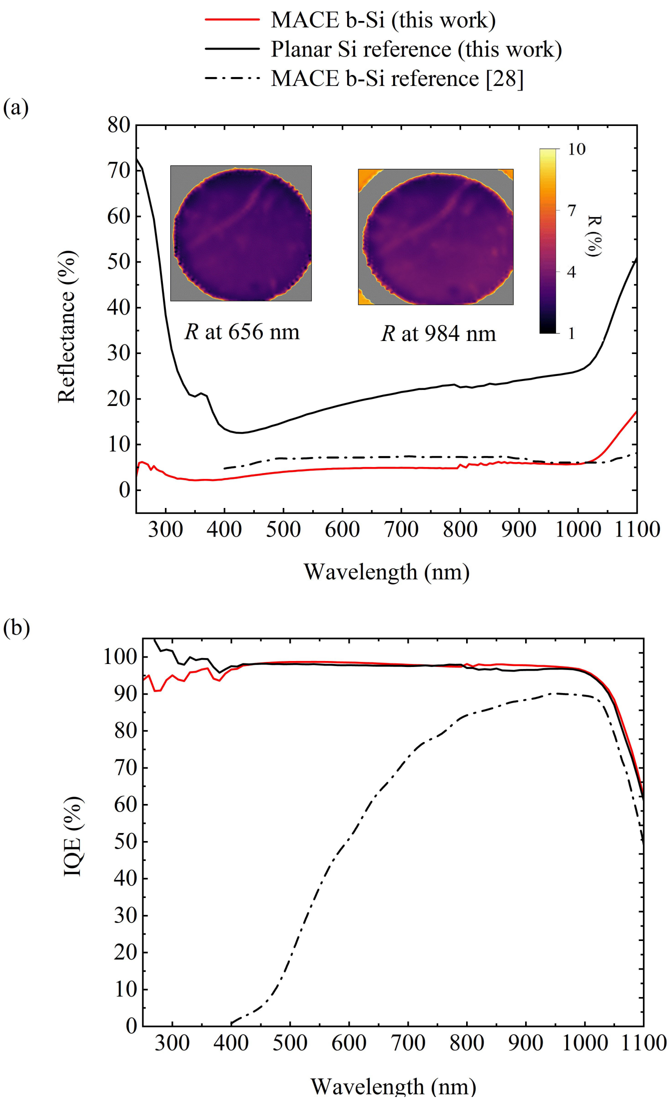

Fig. 3. (a) Total reflectance of MACE b-Si and planar Si p-n photodiodes fabricated in this work, and as a comparison, the reflectance of a state-of-the-art MACE p-n photodiode [28]. Inset: reflectance maps of our 5-mm-diameter MACE b-Si photodiode at the wavelengths of 656 and 984 nm. (b) Corresponding IQE curves.

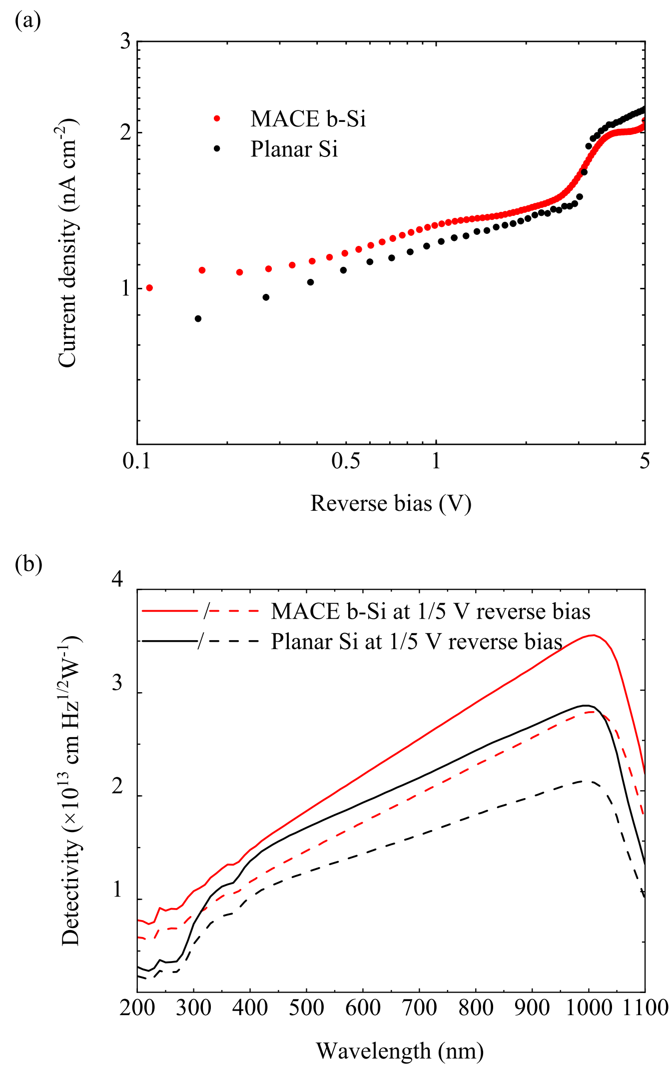

Fig. 4. (a) Dark I–V and (b) specific detectivity of the MACE b-Si and planar Si photodiodes fabricated in this work measured at the reverse bias voltages of 1 and 5 V.

In addition to the spectral responsivity, the final device performance is also affected by dark current [Fig. 4(a)]. These two together determine the sensitivity of the device. In our MACE photodiode, the dark current density measured at 1-V reverse bias is 1.3 nA cm^{-2}, which is comparable to commercial Si photodiodes (≈0.1–10 nA cm^{-2}) [33], [34]. The dark current remains low with increasing reverse bias; e.g., at −5 V, the dark current density of the MACE device is around 2.1 nA cm^{-2}. Zhong et al. [28] did not report the dark current for their MACE photodiode, and therefore, it is not shown here. Interestingly, the dark current of our MACE device is on the same level as the planar reference photodiode. The low dark current means that there cannot be a significant amount of thermal generation centers (defects), and since all generation centers are also recombination centers [35], [36], this result further proves that MACE does not introduce significant metal contamination or other impurities into silicon. This has been a constant debate earlier when the reported leakage currents have been much higher in MACE diodes.

Another important parameter of the photodiode is the sensitivity, which is best described with the so-called specific detectivity that reflects the smallest detectable light intensity and allows the comparison between photodiodes of different sizes. Our MACE photodiode shows the detectivities of 8.0×10^{12} and 3.6×10^{13} Jones (Jones = cm Hz$^{1/2}$ W^{-1}) at the wavelengths of 200 and 1000 nm under a reverse bias voltage of 1 V, respectively [Fig. 4(b)]. Due to its higher responsivity, the MACE photodiode shows higher detectivity and, consequently, higher sensitivity to small light intensities compared with the planar one.

While the MACE photodiode presented here is outperforming the one reported earlier, it is worth noting that there are previous works on b-Si p-n photodiodes textured with more complicated and expensive methods, namely, using plasma etching [24], [25]. Such photodiodes exhibit even higher responsivity (closely following the ideal curve all the way from UV to NIR). However, plasma texturization cannot compete with the simplicity, up-scalability, and cost provided by MACE. Nevertheless, the comparison indicates that there is still room for improvement in the performance of MACE photodiodes. Indeed, as reported in the literature [27], even lower reflectance should be achievable by MACE. Likewise, as seen earlier in Fig. 3(a), the IQE of MACE could be slightly improved by reducing further the surface recombination. Therefore, by proper MACE and ALD process tuning, p-n photodiodes with low-cost and simple b-Si fabrication are realistic without compromising the high device performance.

IV. Conclusion

We have fabricated an MACE p-n photodiode with a record-high responsivity from 200 nm (164.5 mA W^{-1}) to 1100 nm (456.0 mA W^{-1}) with a peak at 1000 nm (731.3 mA W^{-1}). Effective mitigation of reflectance by MACE nanostructures as well as junction and surface recombination by ALD Al_2O_3-induced junction and effective surface passivation, respectively, allowed reaching near ideal performance (EQE close to 100%) over the whole wavelength range. Furthermore, our photodiode demonstrates the possibility to reach low dark currents even with MACE nanotexturing, which, consequently, is seen as the detectivities of 8.0×10^{12} and 3.6×10^{13} Jones at the wavelengths of 200 and 1000 nm at a bias voltage of -1 V, respectively. The high sensitivity also proves the compatibility of the MACE process with conventional p-n photodiode fabrication without introducing contamination issues. Consequently, similar to solar cells, MACE has the potential to reform the photodetector industry by significantly improving device performance with low fabrication costs.

Acknowledgment

The authors would like to thank the provision of facilities and technical support by the Micronova Nanofabrication Centre and the Nanomicroscopy Centre within the OtaNano research infrastructure at Aalto University, Espoo, Finland.

References

[1] Y. Ren and V. Van, "Ultrawide-band silicon microring avalanche photodiode with linear photocurrent-wavelength response," *Photon. Res.*, vol. 9, no. 11, pp. 2303–2308, Nov. 2021, doi: 10.1364/PRJ.437576.

[2] C. Romei, A. D. Fulvio, C. A. Traino, R. Ciolini, and F. d'Errico, "Characterization of a low-cost PIN photodiode for dosimetry in diagnostic radiology," *Phys. Medica*, vol. 31, no. 1, pp. 112–116, Feb. 2015, doi: 10.1016/j.ejmp.2014.11.001.

[3] I. Lee, N. Park, H. Lee, C. Hwang, J. H. Kim, and S. Park, "Systematic review on human skin-compatible wearable photoplethysmography sensors," *Appl. Sci.*, vol. 11, no. 5, p. 2313, Mar. 2021, doi: 10.3390/app11052313.

[4] H. Xu et al., "A simple I-ToF module based on avalanche photodiode," *IEEE Photon. Technol. Lett.*, vol. 33, no. 3, pp. 123–126, Feb. 1, 2021, doi: 10.1109/LPT.2020.3047115.

[5] A. Richter et al., "Design rules for high-efficiency both-sides-contacted silicon solar cells with balanced charge carrier transport and recombination losses," *Nature Energy*, vol. 6, no. 4, pp. 429–438, Apr. 2021, doi: 10.1038/s41560-021-00805-w.

[6] H. Nasser, M. Z. Borra, E. H. Çiftpınar, B. Eldeeb, and R. Turan, "Fourteen percent efficiency ultrathin silicon solar cells with improved infrared light management enabled by hole-selective transition metal oxide full-area rear passivating contacts," *Prog. Photovolt., Res. Appl.*, vol. 30, no. 8, pp. 823–834, Aug. 2022, doi: 10.1002/pip.3510.

[7] K. Chen, O. E. Setala, B. Radfar, U. Kroth, V. Vahanissi, and H. Savin, "Harnessing carrier multiplication in silicon solar cells using UV photons," *IEEE Photon. Technol. Lett.*, vol. 33, no. 24, pp. 1415–1418, Dec. 15, 2021, doi: 10.1109/LPT.2021.3124307.

[8] Z. G. Huang et al., "Large-area MACE Si nano-inverted-pyramids for PERC solar cell application," *Sol. Energy*, vol. 188, pp. 300–304, Aug. 2019, doi: 10.1016/j.solener.2019.06.015.

[9] J. Y.-H. Chai, B. T. Wong, and S. Juodkazis, "Black-silicon-assisted photovoltaic cells for better conversion efficiencies: A review on recent research and development efforts," *Mater. Today Energy*, vol. 18, Dec. 2020, Art. no. 100539, doi: 10.1016/j.mtener.2020.100539.

[10] D. Zhang et al., "Fabrication of inverted pyramid structure for high-efficiency silicon solar cells using metal assisted chemical etching method with $CuSO_4$ etchant," *Sol. Energy Mater. Sol. Cells*, vol. 230, Sep. 2021, Art. no. 111200, doi: 10.1016/j.solmat.2021.111200.

[11] K. P. Sreejith, A. K. Sharma, P. K. Basu, and A. Kottantharayil, "A comprehensive investigation of the potential of metal assisted chemical etched (MACE) nano-textures over conventional micron-sized iso-textures for industrial silicon solar cell applications," *Sol. Energy*, vol. 230, pp. 874–882, Dec. 2021, doi: 10.1016/j.solener.2021.10.035.

[12] S. Zou et al., "Metal-catalyzed chemical etching using DIO_3 as a hole injection agent for efficient submicron-textured multicrystalline silicon solar cells," *Sol. Energy Mater. Sol. Cells*, vol. 227, Aug. 2021, Art. no. 111104, doi: 10.1016/j.solmat.2021.111104.

[13] D. Zhang et al., "Improving the performance of PERC silicon solar cells by optimizing the surface inverted pyramid structure on large-area mono-crystalline silicon wafers," *Mater. Sci. Semicond. Process.*, vol. 138, Feb. 2022, Art. no. 106281, doi: 10.1016/j.mssp.2021.106281.

[14] C. Huo et al., "Metal-assisted chemical etching of silicon in oxidizing HF solutions: Origin, mechanism, development, and black silicon solar cell application," *Adv. Funct. Mater.*, vol. 30, no. 52, Dec. 2020, Art. no. 2005744, doi: 10.1002/adfm.202005744.

[15] P. Zhang et al., "The influence of Ag-ion concentration on the performance of mc-Si silicon solar cells textured by metal assisted chemical etching (MACE) method," *Sol. Energy Mater. Sol. Cells*, vol. 200, Sep. 2019, Art. no. 109983, doi: 10.1016/j.solmat.2019.109983.

[16] G. von Gastrow et al., "Analysis of the atomic layer deposited Al_2O_3 field-effect passivation in black silicon," *Sol. Energy Mater. Sol. Cells*, vol. 142, pp. 29–33, Nov. 2015, doi: 10.1016/j.solmat.2015.05.027.

[17] B. Hoex, J. Schmidt, P. Pohl, M. C. M. van de Sanden, and W. M. M. Kessels, "Silicon surface passivation by atomic layer deposited Al_2O_3," *J. Appl. Phys.*, vol. 104, no. 4, Aug. 2008, Art. no. 044903, doi: 10.1063/1.2963707.

[18] G. Agostinelli et al., "Very low surface recombination velocities on p-type silicon wafers passivated with a dielectric with fixed negative charge," *Solar Energy Mater. Solar Cells*, vol. 90, nos. 18–19, pp. 3438–3443, Nov. 2006, doi: 10.1016/j.solmat.2006.04.014.

[19] J. Ferguson, A. Weimer, and S. George, "Atomic layer deposition of ultrathin and conformal Al_2O_3 films on BN particles," *Thin Solid Films*, vol. 371, nos. 1–2, pp. 95–104, Aug. 2000, doi: 10.1016/S0040-6090(00)00973-1.

[20] T. Niewelt, W. Kwapil, M. Selinger, A. Richter, and M. C. Schubert, "Long-term stability of aluminum oxide based surface passivation schemes under illumination at elevated temperatures," *IEEE J. Photovolt.*, vol. 7, no. 5, pp. 1197–1202, Sep. 2017, doi: 10.1109/JPHOTOV.2017.2713411.

[21] I. T. S. Heikkinen, G. Koutsourakis, S. Wood, V. Vähänissi, F. A. Castro, and H. Savin, "Stability of the surface passivation properties of atomic layer deposited aluminum oxide in damp heat conditions," *AIP Conf. Proc.*, vol. 2147, no. 1, 2019, Art. no. 050003, doi: 10.1063/1.5123852.

[22] K. Chen, T. P. Pasanen, V. Vahanissi, and H. Savin, "Effect of MACE parameters on electrical and optical properties of ALD passivated black silicon," *IEEE J. Photovolt.*, vol. 9, no. 4, pp. 974–979, Jul. 2019, doi: 10.1109/JPHOTOV.2019.2917787.

[23] T. E. Hansen, "Silicon UV-photodiodes using natural inversion layers," *Phys. Scripta*, vol. 18, no. 6, pp. 471–475, Dec. 1978, doi: 10.1088/0031-8949/18/6/025.

[24] M. A. Juntunen, J. Heinonen, V. Vähänissi, P. Repo, D. Valluru, and H. Savin, "Near-unity quantum efficiency of broadband black silicon photodiodes with an induced junction," *Nature Photon.*, vol. 10, no. 12, pp. 777–781, Dec. 2016, doi: 10.1038/nphoton.2016.226.

[25] M. Garin et al., "Black-silicon ultraviolet photodiodes achieve external quantum efficiency above 130%," *Phys. Rev. Lett.*, vol. 125, no. 11, Sep. 2020, Art. no. 117702, doi: 10.1103/PhysRevLett.125.117702.

[26] Y. Zhang, J. Y. Y. Loh, and N. P. Kherani, "Facilely achieved self-biased black silicon heterojunction photodiode with broadband quantum efficiency approaching 100%," *Adv. Sci.*, vol. 9, no. 33, Nov. 2022, Art. no. 2203234, doi: 10.1002/advs.202203234.

[27] K. Kim, B. Ki, H. Bong, K. Choi, and J. Oh, "Ultralow optical and electrical losses via metal-assisted chemical etching of antireflective nanograss in conductive mesh electrodes," *Adv. Opt. Mater.*, vol. 8, no. 15, Aug. 2020, Art. no. 2000143, doi: 10.1002/adom.202000143.

[28] H. Zhong, A. Guo, G. Guo, W. Li, and Y. Jiang, "The enhanced light absorptance and device application of nanostructured black silicon fabricated by metal-assisted chemical etching," *Nanosc. Res. Lett.*, vol. 11, no. 1, p. 322, Dec. 2016, doi: 10.1186/s11671-016-1528-0.

[29] J. Heinonen et al., "Results on radiation hardness of black silicon induced junction photodetectors from proton and electron radiation," *Nucl. Instrum. Methods Phys. Res. A, Accel. Spectrom. Detect. Assoc. Equip.*, vol. 977, Oct. 2020, Art. no. 164294, doi: 10.1016/j.nima.2020.164294.

[30] S. Liu et al., "Ultrasensitive water-processed monolayer photodetectors," *Chem. Sci.*, vol. 2, no. 4, p. 796, 2011, doi: 10.1039/c0sc00488j.

[31] V. Mackowiak, J. Peupelmann, Y. Ma, and A. Gorges, "NEP—Noise equivalent power," Thorlabs, Newton, NJ, USA, White Paper, 2015. [Online]. Available: https://www.thorlabschina.cn/images/TabImages/Noise_Equivalent_Power_White_Paper.pdf

[32] S. Kolodinski, J. H. Werner, T. Wittchen, and H. J. Queisser, "Quantum efficiencies exceeding unity due to impact ionization in silicon solar cells," *Appl. Phys. Lett.*, vol. 63, no. 17, pp. 2405–2407, Oct. 1993, doi: 10.1063/1.110489.

[33] Hamamatsu Photonics, Hamamatsu, Japan. (Aug. 2022). *Selection Guide/Si Photodiodes*. [Online]. Available: https://www.hamamatsu.com/content/dam/hamamatsu-photonics/sites/documents/99_SALES_LIBRARY/ssd/si_pd_kspd0001e.pdf

[34] OSI Optoelectronics, Hawthorne, CA, USA. *Photoconductive Series Datasheet*. Accessed: Dec. 6, 2022. [Online]. Available: https://www.osioptoelectronics.com/Libraries/Datasheets/Photoconductive-Photodiodes.sflb.ashx

[35] H. M. Ayedh et al., "Fast wafer-level characterization of silicon photodetectors by photoluminescence imaging," *IEEE Trans. Electron Devices*, vol. 69, no. 5, pp. 2449–2456, May 2022, doi: 10.1109/TED.2022.3159497.

[36] D. K. Schroder, "Carrier lifetimes in silicon," *IEEE Trans. Electron Devices*, vol. 44, no. 1, pp. 160–170, Jan. 1997, doi: 10.1109/16.554806.

Kexun Chen received the D.Sc. (Tech.) degree in physical science and technology from Soochow University, Suzhou, China, in 2018.

He is currently working as a Postdoctoral Researcher with the Department of Electronics and Nanoengineering, Aalto University, Espoo, Finland. His research interests include surface texturization, especially nanostructured silicon, and surface passivation in silicon photovoltaics.

Olli E. Setälä received the M.Sc. (Tech.) degree in electronics and nanotechnology from Aalto University, Espoo, Finland, in 2020, where he is currently pursuing the Ph.D. degree in photonics and nanotechnology.

His current research focuses on high-sensitivity photon and particle detection with photodiodes as well as texturization and passivation of silicon surface.

Xiaolong Liu received the Ph.D. degree in optics from Fudan University, Shanghai, China, in 2020.

He is currently working as a Postdoctoral Researcher at the Department of Electronics and Nanoengineering, Aalto University, Espoo, Finland. His current work focuses on micro- and nanotextured silicon and its application in optoelectronic devices.

Behrad Radfar (Graduate Student Member, IEEE) received the B.Sc. degree in electrical and electronics engineering from the University of Tehran, Tehran, Iran, in 2014, and the M.Sc. degree in micro- and nanotechnology from Middle East Technical University, Ankara, Turkey, in 2019. He is currently pursuing the Ph.D. degree in electronics and nanoengineering with Aalto University, Espoo, Finland.

His research interests include surface modification, laser texturing, and silicon-based photovoltaics

Toni P. Pasanen received the D.Sc. (Tech.) degree in micro- and nanosciences from Aalto University, Espoo, Finland, in 2019.

He worked as a Postdoctoral Researcher with Aalto University, until January 2023. He is currently working on highly sensitive photodiodes as a Senior Project Engineer at ElFys, Inc., Espoo.

Michael D. Serué received the M.Sc. (Tech.) degree in micro- and nanosciences from Aalto University, Espoo, Finland.

His background is in silicon solar cell defect research. He has been working on customer integration and demonstration projects, and photodiode fabrication and characterization as a Project Engineer at ElFys, Inc., Espoo, since 2019.

Juha Heinonen received the D.Sc. (Tech.) degree in micro- and nanosciences from Aalto University, Espoo, Finland, in 2022.

He is one of the co-founders of ElFys, Inc., Espoo, where he is currently working as a Project Manager. His research interests include black silicon, atomic layer deposition and their applications in photodetectors.

Hele Savin received the D.Sc. (Tech.) degree in semiconductor technology from the Helsinki University of Technology, Espoo, Finland, in 2005.

She is currently a Professor with the Department of Electronics and Nanoengineering, Aalto University, Espoo. Her current research interests focus on photonic devices, especially photon detection and solar cells, nanofabrication methods, and defect engineering in group-IV materials.

Ville Vähänissi received the D.Sc. (Tech.) degree in semiconductor technology from Aalto University, Espoo, Finland, in 2016.

He is currently working as a Staff Scientist at the Department of Electronics and Nanoengineering, School of Electrical Engineering, Aalto University. His research interests include defect engineering in silicon, especially photovoltaics, as well as atomic layer deposition, and its various applications in semiconductor devices.